CRYSTAL GROWTH & DESIGN

pubs.acs.org/crystal

Article

[2 + 2] Photodimerization of Sulfonate Derivative of *trans*-Cinnamic Acid: Kinetics Study Using Solid State ^{13}C NMR and Hybrid Material Inclusion

Varun Kumar, Luca Fusaro, Carmela Aprile, Koen Robeyns, and Yann Garcia*

Cite This: *Cryst. Growth Des.* 2020, 20, 7850−7861

Read Online

ACCESS | Metrics & More | Article Recommendations | Supporting Information

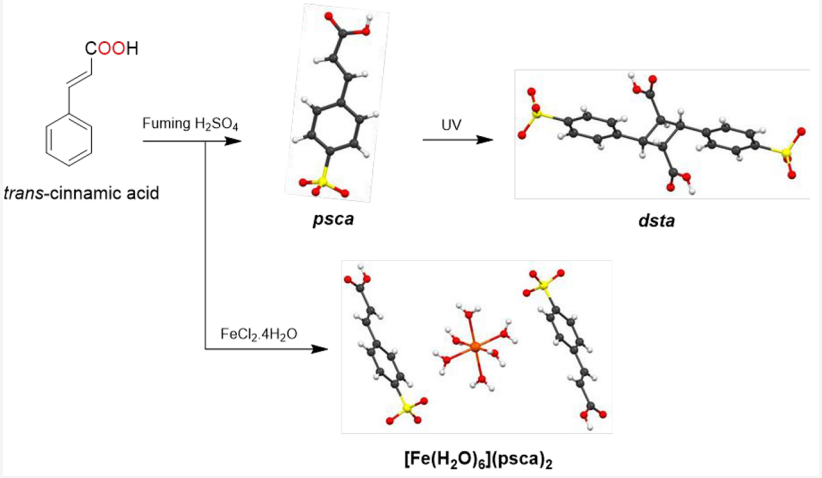

ABSTRACT: A sulfonic acid, namely *p*-sulfocinnamic acid (***psca***), has been synthesized and characterized spectroscopically as well as by single crystal X-ray diffraction. The crystal structure of ***psca*** reveals that it fulfils Schmidt's topochemical rules for [2 + 2] photodimerization and the molecules to be dimerized are arranged in head-to-tail manner, confirming ***psca*** to be an α-type polymorph. The [2 + 2] photodimerization of ***psca*** has been monitored using solid state ^{13}C CP-MAS NMR spectroscopy which certifies a 100% photoconversion to yield to 4,4′-disulfonate-truxillic acid (***dsta***). The Avrami constant, $n = 1.8(1)$, derived from the Johnson−Mehl−Avrami−Kolmogorov (JMAK) model, indicates that [2 + 2] photodimerization proceeds with a decreasing nucleation rate and formation of ***dsta*** occurs through a one-dimensional heterogeneous linear growth. The crystal structure of ***dsta*** unveils it to be a centrosymmetric molecule. The solvent molecules present in the crystal lattice interconnect all truxillic acid molecules through a 3D hydrogen bonding network. Guest insertion of ***psca*** into a selected inorganic host-network, as a proof of concept for hybrid materials design, provided $[Fe(H_2O)_6](psca)_2{\cdot}2H_2O$, which has been structurally characterized and investigated by ^{57}Fe Mössbauer spectroscopy.

INTRODUCTION

Photoresponsive molecules undergo definite structural or conformational changes when irradiated with light of certain wavelengths. These structural changes often cause changes in their physical and chemical properties, making the photoresponsive molecules potential candidates for optical data storage and display devices.[1] The response to light irradiation may include *keto*−*enol* tautomerization,[2] *cis*−*trans* isomerization,[3] cycloaddition,[4] etc. Molecules exhibiting photoinduced [2 + 2] intercycloaddition between two unsaturated molecules represent a fascinating substance class. In particular, molecules based on *trans*-cinnamic acid undergoing [2 + 2] photocycloaddition in the solid state at ambient conditions have attracted considerable interest.[5] This synthetic method represents an economical and environmentally friendly approach to produce covalent bonds in organic molecules, which prevent exposure to harmful solvents usually employed in classic organic chemistry.[6] The [2 + 2] photocycloaddition of *trans*-cinnamic acid under the influence of UV light has been studied for more than a century.[7] Since the first systematic study on [2 + 2] photodimerization of the original molecule

Received: August 16, 2020
Revised: October 29, 2020
Published: November 17, 2020

https://dx.doi.org/10.1021/acs.cgd.0c01149
Cryst. Growth Des. 2020, 20, 7850−7861

and its derivatives,[8] many studies have aimed to control,[9] design,[10−12] and understand the mechanism of the solid state photoreaction.[13,14] Despite the irreversible nature of the photoconversion in *trans*-cinnamic acid, it still holds a suitable importance as a functional material because the photoreaction proceeds in the solid state at room temperature and ambient pressure, thus opening up the possibility for *trans*-cinnamic acid to be included as a guest molecule into hybrid materials or polymers, to generate new functional materials.

There are two known variants of photoresponsive *trans*-cinnamic acid, namely α-type and β-type.[15] In α-type, the two monomers that undergo photodimerization are arranged in a head-to-tail manner whereas in β-type, the monomers are arranged in head-to-head manner as shown in Scheme 1.

Scheme 1. Two Variants of *trans*-Cinnamic Acid and Their Photodimerization Products

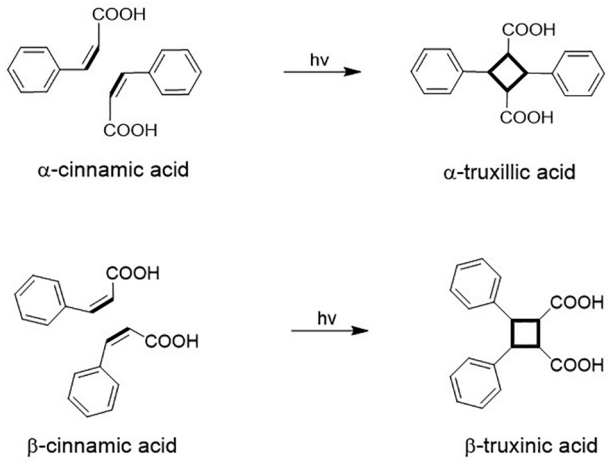

Schmidt et al. postulated the fundamental rules of topochemical solid state [2 + 2] photodimerization in *trans*-cinnamic acid[15] to occur as follows: (i) the distance between the concerned vinyl bonds (d) should be $d \leq 4.2$ Å and (ii) the two vinyl bonds should be parallel to each other in order to have a good overlap of π-orbitals (Scheme 2). If these rules are

Scheme 2. Structural Conditions for Vinyl Bonds to Undergo [2 + 2] Photodimerization

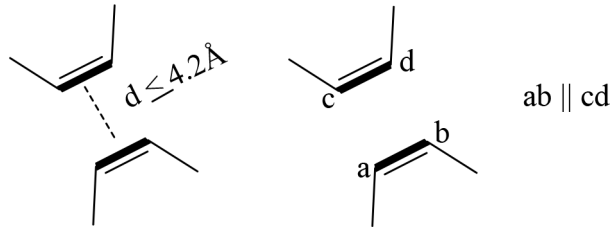

met, the photodimerization is most likely to proceed. Some reports, however, violate these postulates.[16−18] For instance, Murthy while studying derivatives of *trans*-cinnamic acid found that the distance between vinyl bonds of 4-hydroxy-3-nitrocinnamate was d = 3.7 Å and yet it exhibited no photodimerization.[16] Nonetheless, it is still best to keep the original Schmidt's postulates in mind while designing new molecules.

In this paper, we study the [2 + 2] photodimerization properties of a sulfonate derivative of α-*trans*-cinnamic acid, called *p*-sulfocinnamic acid (***psca***). The photoreaction depicted in Scheme 3 was monitored by using solid state ^{13}C CP-MAS

Scheme 3. Reaction Scheme of [2 + 2] Photodimerization of *p*-Sulfocinnamic Acid (*psca*) to 4,4′-Disulfonate-truxillic Acid (*dsca*)

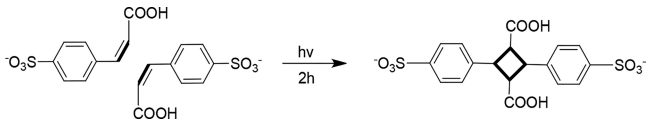

NMR spectroscopy. The kinetics of the reaction were described using the Johnson−Mehl−Avrami−Kolmogorov (JMAK) model of nucleation and growth for solids.[19−21] Alongside kinetics study, a thorough characterization of *p*-sulfocinnamic acid (***psca***) and its new photoproduct, 4,4′-disulfonate-truxillic acid (***dsta***) including their crystal structures and infrared spectroscopy investigation are also described herein. This article is critical as it studies and identifies the photodimerization properties of ***psca*** in detail. Being photoresponsive and possessing a negative charge, ***psca*** holds the potential to be included in a variety of organic blends, and inorganic lattices, including cationic metal complexes as a counteranion.[22] This strategy will allow proposal of a novel generation of photoresponsive hybrid materials. As a proof of concept, we have successfully inserted ***psca*** into a hexa-aqua-iron complex $[Fe(H_2O)_6](psca)_2{\cdot}2H_2O$, whose crystal structure and ^{57}Fe Mössbauer investigation are also presented.

EXPERIMENTAL SECTION

Materials and Characterization Techniques. *trans*-Cinnamic acid and 20% fuming sulfuric acid were purchased from Acros-organics. $FeCl_2{\cdot}4H_2O$ and acetic acid were purchased from Sigma-Aldrich. All the chemicals were used as received without further purification. Fourier-transform infrared spectra were recorded on a Shimadzu FTIR-8400S instrument using KBr pellets. Solution-state ^{13}C NMR spectra were recorded at room temperature on a Bruker Avance II 300 MHz spectrometer. The samples were dissolved in DMSO-d_6. Chemical shifts (δ) are reported in parts per million and were referenced to the residual signal of the solvent (δ = 39.52 ppm). Mass spectral data were recorded on a Q-Exactive mass spectrometer from Thermo Fisher Scientific. Powder XRD analysis was done on a D8 Advanced diffractometer from Bruker. The diffractogram was recorded using Cu Kα radiation (0.15406 nm) and linkeye XE-T detector (Bruker) in the 5−70° (2θ) range with an increment of 0.0015° and an integration time of 0.15 s. Solid-state ^{13}C CP-MAS NMR spectra were recorded at room temperature on a Bruker Avance 500 MHz spectrometer operating at 11.7 T (500 MHz for ^{1}H and 125 MHz for ^{13}C). All the spectra were obtained using a 4 mm CP-MAS probe with a spinning frequency of 5 kHz, contact time of 2 ms and relaxation delay of 300 s. The chemical shift scale was referenced externally to solid adamantane (38.48 and 29.45 ppm) with respect to TMS. ^{57}Fe Mössbauer spectra were recorded at room temperature in transmission geometry mode with a constant acceleration mode conventional Wissel Mössbauer spectrometer equipped with a ^{57}Co-(Rh) radioactive source provided by Cyclotron Ltd., a Reuter Stokes proportional counter detector and a Wissel CMCA-550 multichannel analyzer. All isomer shifts in Mössbauer spectra are given respective to α-Fe.

Syntheses. *p-Sulfocinnamic Acid (psca).* A 5.0 g portion of finely ground *trans*-cinnamic acid was added in small amounts to 8.0 mL of 20% fuming sulfuric acid kept in an ice−water bath. After complete addition, the reaction mixture was vigorously stirred at room temperature for 30 min. Thereafter, the thick brown reaction mixture was heated in an oil bath set at 60 °C for 2 h. The dark brown

https://dx.doi.org/10.1021/acs.cgd.0c01149
Cryst. Growth Des. 2020, 20, 7850−7861

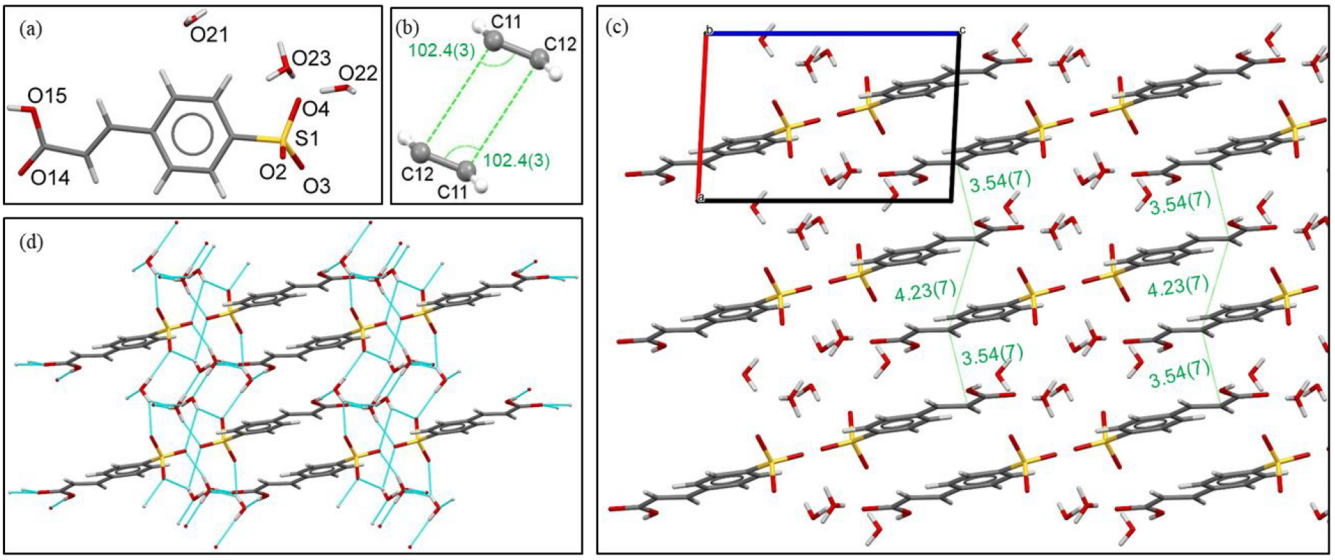

Figure 1. Crystal structure of ***psca***. (a) Asymmetric unit, (b) angles between vinyl bonds of two molecules to be dimerized, (c) crystal packing when viewed along the *b*-axis, (d) hydrogen bonding network in ***psca***, showing the hydrogen bonds as dashed cyan lines.

solution was then cooled down to room temperature and added to 30 mL of ice water with vigorous stirring. The resulting solution was then allowed to stand still for a period of 1−2 days. After 2 days, crystals of ***psca*** started to separate from the reaction mixture. These crystals were filtered using a Buchner funnel and washed with diethyl ether. At last, the product was recrystallized from distilled water to obtain single crystals. Yield: 59% (4.52 g). FTIR (KBr, cm^{-1}): 1679 cm^{-1} (C═O), 1644 (C═C), 1311 (asym S═O), 1123 (sym S═O), 824 (S−O). ^{1}H NMR [300 MHz, DMSO-d_6, δ (ppm)] 7.66 (2H, d), 7.62 (2H, d), 7.57 (1H, d), 6.53 (1H, d). MS (FTMS − pAPCI): m/z 227.00 [M^+].

*4,4′-Disulfonate-truxillic Acid (**dsta**).* The solid state [2 + 2] photodimerization was performed with a broad UV wavelength fluorescent 15 W Phillips lamp. A 105 mg portion of crystallized ***psca*** was finely ground and spread evenly on a watch glass, thereafter ***psca*** was irradiated for 2 h to obtain ***dsta***. During the irradiation, ***psca*** was thoroughly mixed using a spatula at regular intervals of 20 min in order to ensure maximum and homogeneous light exposure. After irradiation, the photoproduct was recrystallized from aqueous acetic acid to obtain crystals suitable for single crystal-XRD. FTIR (KBr, cm^{-1}): 1712 (C═O), 1313 (asym. S═O), 1126 (sym. S═O), 844 (S−O). ^{1}H NMR [300 MHz, DMSO-d_6, δ (ppm)] 7.57 (4H, d), 7.34 (4H, d), 4.29 (2H, m), 3.82 (2H, m). MS (FTMS + pESI): m/z 227.00 [M^+].

*[Fe(H$_2$O)$_6$)](**psca**)$_2$·2H$_2$O.* The synthesis was done following our recently reported procedure.[23] Single crystals were obtained upon recrystallization from distilled H_2O. Yield: 57% (6.25 g). FTIR (KBr, cm^{-1}): 1695 cm^{-1} (C═O), 1631 (C═C), 1314 (asym S═O), 1126 (sym S═O), 807 (S−O). Elemental analysis calculated for $FeC_{18}O_{18}H_{30}S_2$: C, 33.04; H, 4.62; S, 9.80. Found: C, 33.04; H, 4.60; S, 9.79.

Single Crystal X-ray Diffraction. Single crystal X-ray diffraction (SXRD) data for ***psca*** was collected at 100 K on an Agilent Supernova diffractometer, equipped with an Atlas CCD detector, using Mo−Kα radiation (λ = 0.71073 Å). Intensity data for ***dsta*** and [Fe(H$_2$O)$_6$]-(***psca***)$_2$·2H$_2$O were measured on a MAR345 image plate detector using Mo−Kα radiation (λ = 0.71073 Å), generated by a Rigaku UltraX 18S generator with a Xenocs Fox3D mirror. ***dsta*** was measured at room temperature and [Fe(H$_2$O)$_6$](***psca***)$_2$ was flash cooled to 150 K prior to data collection. Data reduction and integration was performed by CrysAlis^{Pro}.[24] The selected crystal of ***psca*** and [Fe(H$_2$O)$_6$](***psca***)$_2$·2H$_2$O were found to be twinned and both twin domains were integrated simultaneously. All the structures were solved by Direct Methods, SHELXT,[25] and refined by full-matrix least-squares minimization on F^2 using SHELXL2014/7.[26] Non-hydrogen atoms were refined anisotropically and hydrogen atoms were placed in calculated positions and refined in riding mode with isotropic temperature factors fixed at 1.2 times U_{eq} of the parent atoms (1.5 for H_2O molecules). In [Fe(H$_2$O)$_6$](***psca***)$_2$·2H$_2$O, the carboxylic end was found to be disordered over two sites (66/34 ratio), and the minor part was refined to be geometrically similar to the major part. Isotropic and rigid bond restraints were applied to the disordered parts. H atoms on the water molecules were located in the difference maps, idealized and refined as rigid groups allowing rotation around the oxygen atom. The hydrogens of the hydronium ions in ***psca*** and ***dsta*** were located in the difference maps, and distance restraints were applied for the O−H bonds; no angle or bond angle restraints were set.

psca and [Fe(H$_2$O)$_6$](***psca***)$_2$·2H$_2$O were found to be twinned, during data processing and both twin domains were simultaneous integrated. The subsequent refinement cycles were performed against HKLF5 formatted data.

The crystallographic and refinement data for all the complexes is summarized in Table S1 in the Supporting Information. Ortep representations of ***psca***, ***dsta***, and [Fe(H$_2$O)$_6$](***psca***)$_2$·2H$_2$O are shown in Figures S1−3, respectively. CCDC 2015099−2015101 for ***psca***, ***dsta***, and [Fe(H$_2$O)$_6$](***psca***)$_2$·2H$_2$O, respectively, contain the supplementary crystallographic data for these compounds and can be obtained free of charge from the Cambridge Crystallographic Data Centre via www.ccdc.cam.ac.uk/structures.

RESULTS

Synthesis and Crystallization. The synthesis of ***psca*** was done following a modified procedure after Moore and Tucker.[27] The addition of *trans*-cinnamic acid into fuming sulfuric acid was done slowly and carefully as the reaction was highly exothermic, using an ice−water bath to control the reaction temperature. After complete addition, the reaction mixture was vigorously stirred to not allow the formation of lumps because the reaction mixture gets very viscous with increasing *trans*-cinnamic acid concentration. After the complete addition and ensuring that no more fumes were coming out of the reaction flask, the reaction mixture was heated at 60 °C to speed up the sulfonation process. At this point, the reaction mixture appears as a clear dark-brown thick solution indicating the completion of the sulfonation process.

https://dx.doi.org/10.1021/acs.cgd.0c01149
Cryst. Growth Des. 2020, 20, 7850−7861

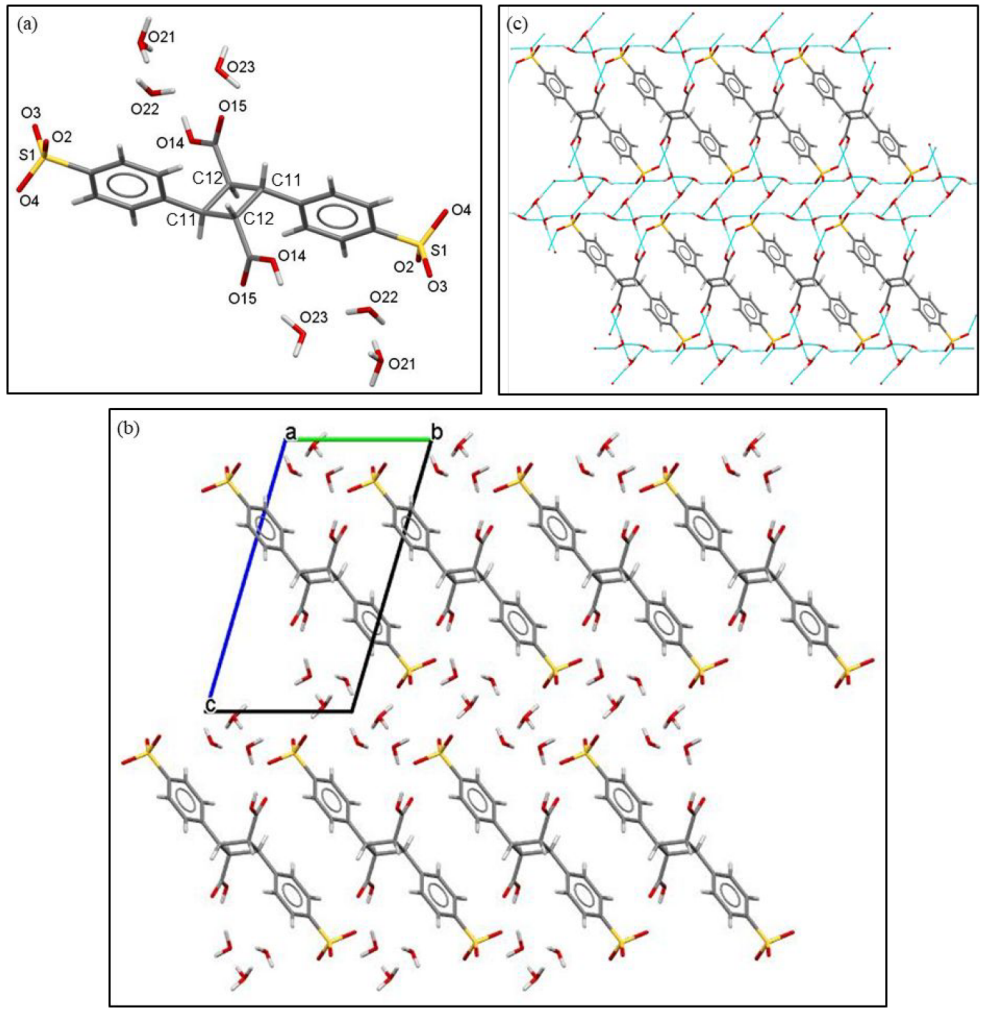

Figure 2. Crystal structure of ***dsta***. (a) Formula unit, (b) crystal packing when viewed along the *a*-axis, (c) hydrogen bonding network in ***dsta***, showing the hydrogen bonds as dashed cyan lines.

The reaction mixture was poured slowly into ice cold water, with continuous stirring to separate ***psca*** from the reaction mixture. If stirring was not maintained while addition, it would lead to desulfonation of ***psca*** back to *trans*-cinnamic acid. After separation, ***psca*** was filtered and washed with diethyl ether to remove the excess of sulfuric acid. Finally, ***psca*** was recrystallized from distilled water to obtain single crystals suitable for single crystal-XRD. The solid state [2 + 2] photodimerization of ***psca*** was performed with a broad UV wavelength fluorescent 15 W lamp. The sample was finely ground and mixed thoroughly at regular intervals to have maximum exposure to UV light irradiation. The dimer ***dsta*** was recrystallized from 50% aqueous acetic acid to obtain single crystals for crystal structure determination. The guest insertion of ***psca*** within a hexaaqua Fe(II) complex was successfully carried out, leading to an aqua iron complex, $[Fe(H_2O)_6](psca)_2{\cdot}2H_2O$. The synthesis of $[Fe(H_2O)_6](psca)_2{\cdot}2H_2O$ was done *in situ* in the sulfonation reaction mixture of *trans*-cinnamic acid. After the completion of the sulfonation reaction, instead of separating out ***psca***, $FeCl_2{\cdot}4H_2O$ was added in excess. $[Fe(H_2O)_6](psca)_2{\cdot}2H_2O$ started to precipitate out within 5 min of stirring. The precipitate was filtered and recrystallized from distilled water to obtain single crystals.[23]

Single Crystal X-ray Diffraction. *Crystal Structure of p-Sulfocinnamic Acid (**psca**).* ***psca*** has a triclinic structure and crystallizes in the $P\bar{1}$ space group. The asymmetric unit comprises one molecule of *p*-sulfocinnamic acid along with two lattice water molecules, and one hydronium ion as shown in Figure 1a. ***psca*** crystallized as a hydronium salt of *p*-sulfocinnamic acid due to highly acidic nature of the sulfonic group which readily loses a hydrogen ion. Figure 1c represents the crystal packing of ***psca*** when viewed along the *b*-axis. In a plane, the molecules arranged themselves in pairs forming a dimeric motif with sulfonate groups facing to each other. Each molecule in the dimeric motif is within the allowed distance for photodimerization with their neighboring molecules situated either below or above them. The molecules that are to undergo photodimerization are stacked in head-to-tail manner in two parallel planes, making ***psca*** an α-type polymorph. The distance between vinyl bonds of these stacked molecules is 3.54(7) Å which is well within the limits of 4.2 Å for photodimerization. Interestingly, another pair of head-to-tail stacked molecules whose vinyl bonds are 4.23(7) Å apart is also spotted in the crystal packing as shown in Figure 1c. Such a distance lies at the uppermost allowed limit of Schmidt's postulates. Thus, this other vinyl pair also holds the potential to undergo photodimerization. However, the vinyl pair which

https://dx.doi.org/10.1021/acs.cgd.0c01149
Cryst. Growth Des. 2020, 20, 7850−7861

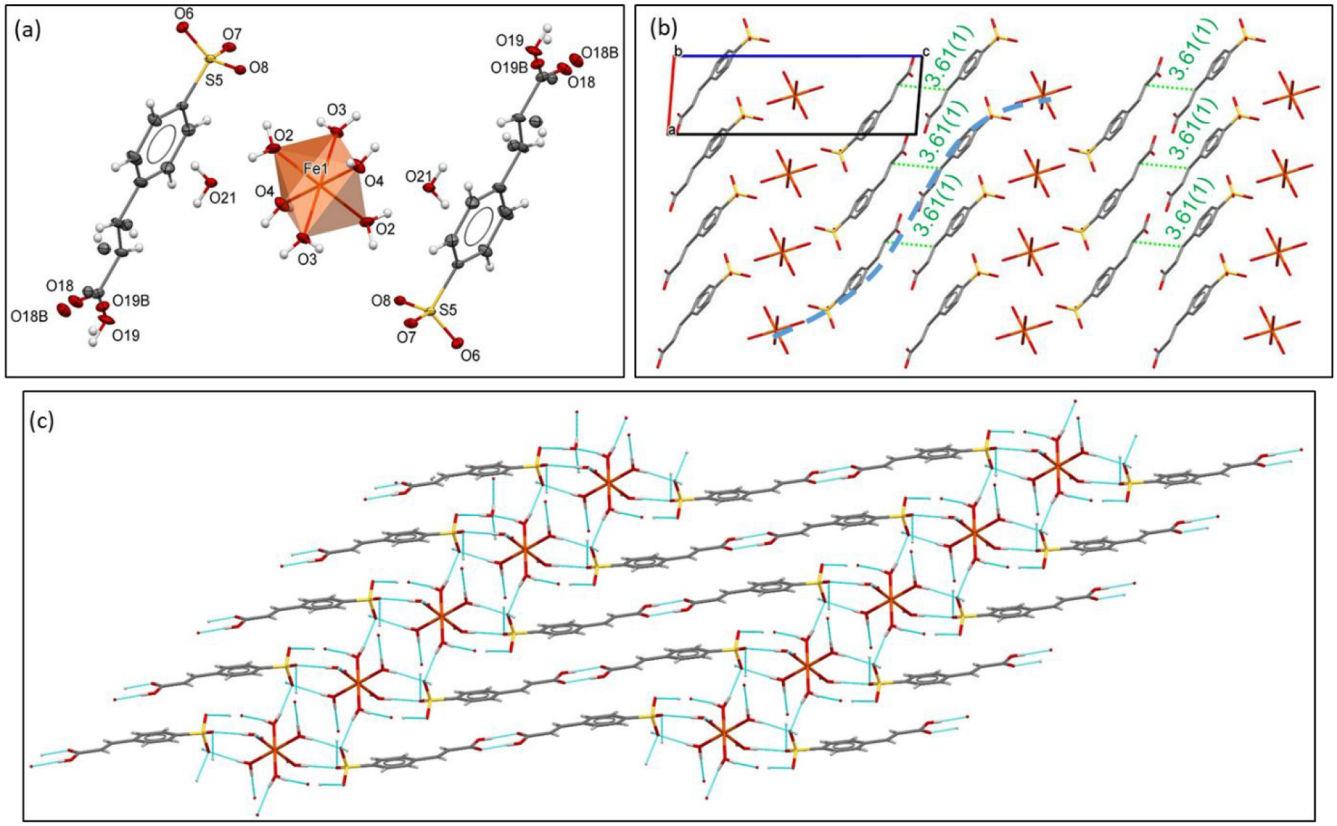

Figure 3. Crystal structure of $[Fe(H_2O)_6](psca)_2{\cdot}2H_2O$. (a) Formula unit, showing thermal displacement ellipsoids at the 30% probability level. The disorder of the vinyl and carboxylic group is shown by the corresponding atom color. (b) Crystal packing when viewed along the *b*-axis. Hydrogen atoms and solvent molecules are removed for clarity. (c) H-bonding network in the crystal lattice which cyan lines representing hydrogen bonds.

is 3.54(7) Å apart is the most likely to undergo photodimerization based on the minimum molecular movement criteria. Therefore, we shall only focus on the vinyl pairs with the shortest distance, i.e. the ones with 3.54(7) Å. A closer look at the vinyl bonds of stacked molecules is given in Figure 1b, where it can be clearly seen that two vinyl bonds have the opposite equal angles, making them parallel to each other. The torsion angle, τ, between the two vinyl bonds is 0° which ensures a maximum overlap between π-orbitals. The crystal water occupies space between the dimeric motifs close to the oxygen rich sulfonate and carboxylate groups. Consequently, multiple hydrogen bonds between the lattice waters and oxygen atoms of sulfonate and carboxylate groups with O(H)···O distances in the range of 2.46(5)−3.14(5) Å are observed. All D−H···A parameters in ***psca*** such as distances, angles, and type of interactions are summed up in Table S2. This strategic position of solvent molecules allow them to form a 3D hydrogen bonding network in the crystal lattice as shown in Figure 1d where cyan bonds represent hydrogen bonds. No aromatic interactions are seen in the crystal packing as the rings are too distant apart.

*Crystal Structure of 4,4′-Dislufonate-truxillic Acid (**dsta**).* ***dsta*** also crystallizes in the triclinic space group $P\bar{1}$. The formula unit is comprised of one molecule of 4,4′-disulfonate-truxillic acid along with four water molecules, and two hydronium ions as shown in Figure 2a; this also reveals the presence of cyclobutane ring with carboxylic groups at opposite ends confirming the success of the [2 + 2] photodimerization reaction of ***psca***. The cyclobutane ring connects two phenyl rings which are parallel to each other and lie in different planes. As a result of ***psca*** being an α-polymorph, sulfonate groups in ***dsta*** occupy positions opposite to each other at each phenyl ring. ***dsta*** is located on an inversion center, as a result the asymmetric unit of ***dsta*** comprises only half of the formula unit. The cyclobutane ring is completely planar as expected for the centro-symmetrical ring substitution.[28] The C−C bond lengths and ∠C−C−C bond angles in cyclobutane ring (C11−C12 = 1.59(4) Å, C12−C11 = 1.55(3) Å, ∠C11−C12−C11 = 90.4(2)°, ∠C12−C11−C12 = 89.6 (2)°) show that the ring slightly deviates from the square geometry.

Figure 2b represents the crystal packing of ***dsta***. A closer inspection of the crystal packing unveils that both sulfonate groups and carboxylic groups on their respective ends in a molecule have identical environments in the crystal packing, thanks to the centro-symmetry of ***dsta***. An extensive hydrogen bond network is formed, where the carboxylic acid proton interacts with the sulfonate group, providing a double interaction on both sides of the molecules along the *b*-axis (Figure 2c). The water and hydronium molecules are situated in layers, with extensive linking between them as well as with the sulfonate and carboxylic acid groups forming a strong 3D hydrogen bonding network as shown in Figure 2b. The O(H)···O distances in hydrogen bonds between H_2O molecules and oxygen atoms of sulfonate and carboxylate groups are in the range of 2.5(3)−2.88(3) Å. See Table S2 for all hydrogen bonding parameters.

https://dx.doi.org/10.1021/acs.cgd.0c01149
Cryst. Growth Des. 2020, 20, 7850−7861

*Crystal Structure of Hexaaqua Iron(II) Sulfocinnamic Acid [Fe(H$_2$O)$_6$](**psca**)$_2$·2H$_2$O.* The hexaaquairon complex, [Fe(H$_2$O)$_6$](***psca***)$_2$·2H$_2$O, crystallizes in the $P\bar{1}$ space group, which is remarkably the same as for ***psca*** and ***dsta***. Figure 3a represents the formula unit and unit cell comprised of one Fe(II) ion coordinated to six water molecules, two molecules of *p*-sulfocinnamic acid as anions, and two lattice water molecules. Each Fe(II) ion is counter balanced by two negatively charged *p*-sulfocinnamic acid anions to maintain charge neutrality in the crystal lattice. The Fe(II) ion exhibits a near perfect octahedral geometry, with quadratic elongation of 1.001.[29] The bond angles in the octahedron are found to be only slightly deviated from right angles, with a distortion parameter $\Sigma = 18.1°$. The Fe−N bond lengths which are of the order of 2.1−2.2 Å indicate [Fe(H$_2$O)$_6$](***psca***)$_2$·2H$_2$O to be a high-spin (HS) complex.[30] Figure 3b shows the crystal packing arrangement in [Fe(H$_2$O)$_6$](***psca***)$_2$·2H$_2$O along the *b*-axis. There are two *p*-sulfocinnamic acid anions which lie in between two Fe(II) ions. The distance between vinyl bonds of these two anions is 3.61(1) Å which is well within the limit for photodimerizable distance. Also the torsion angle, τ between the two vinyl bonds is 0° which provides for a maximum overlap of the π-orbitals. Hence there is a possibility that [Fe(H$_2$O)$_6$](***psca***)$_2$·2H$_2$O could be a photoresponsive complex. The *p*-sulfocinnamic acid molecules are slightly bent. If we follow the dashed blue curve in Figure 3b, the molecules seem to form a wavelike pattern which propagates from one Fe(II) to another Fe(II) ion. The bent shapes of *p*-sulfocinnamic acid molecules are responsible for these waveslike patterns. These patterns are more clearly shown from a different angle in Figure 3c, which also represents the hydrogen-bonding network in the crystal packing. The two *p*-sulfocinnamic acid molecules are linked together through hydrogen bonds from carboxylic groups and act as a bridge along with H$_2$O molecules between two Fe(II) ions. In fact, all the Fe(II) ions in the lattice are interconnected with each other through hydrogen bonding, engaging all of the eight water molecules. The O(H)···O distances in hydrogen bonds between H$_2$O molecules and oxygen atoms of sulfonate and carboxylic groups are in the range of 2.23(3)−2.86(4) Å; see Table S2 for more details.

^{57}Fe Mössbauer Spectroscopy. The ^{57}Fe Mössbauer spectrum recorded at room temperature and in air of [Fe(H$_2$O)$_6$](***psca***)$_2$·2H$_2$O (Figure 4) was fitted to the sum of Lorentzian lines by a least-squares refinement using Recoil 1.05 Mössbauer Analysis Software (Table 1).[31] The red doublet at isomer shift of $\delta = 1.26$ mm/s shows a quadrupole splitting of $\Delta E_Q = 3.18$ mm/s, which is characteristic of Fe(II) HS ions. The large quadrupole splitting arises from electric field gradient in [Fe(H$_2$O)$_6$](***psca***)$_2$·2H$_2$O which in turn is caused by distorted octahedron environment of Fe(II).[32] As expected from SXRD, [Fe(H$_2$O)$_6$](***psca***)$_2$·2H$_2$O is indeed an HS compound, as coordinated water molecules contribute toward the weak ligand field.

The hyperfine parameters obtained for Fe(II) sites of [Fe(H$_2$O)$_6$](***psca***)$_2$·2H$_2$O are similar the one obtained by DeBenedetti et al. for a ferrous ion with same coordination sphere, [Fe(H$_2$O)$_6$]SO$_4$·H$_2$O.[33] Alongside the red doublet, a yellow doublet with an isomer shift, $\delta = 0.14$ mm/s and quadrupole splitting of $\Delta E_Q = 0.43$ mm/s was also observed in the spectrum. The parameters obtained correspond to the presence of Fe(III) HS ions and suggest that [Fe(H$_2$O)$_6$](***psca***)$_2$·2H$_2$O tends to oxidize over time under ambient conditions.

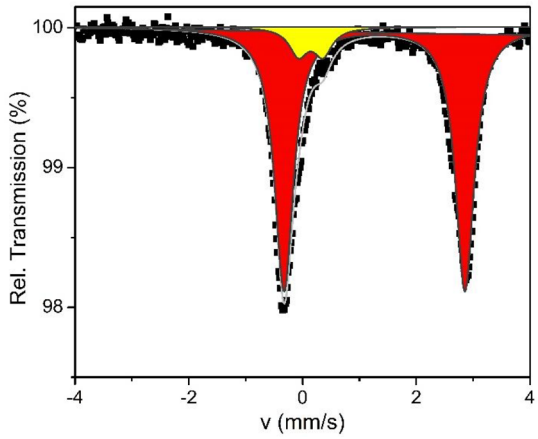

Figure 4. ^{57}Fe Mössbauer spectrum of [Fe(H$_2$O)$_6$](***psca***)$_2$·2H$_2$O at room temperature.

Table 1. ^{57}Fe Mössbauer Parameters [Fe(H$_2$O)$_6$](*psca*)$_2$·2H$_2$O at 298 K[a]

sites	δ (mm/s)	ΔE_Q (mm/s)	$\Gamma/2$ (mm/s)	fraction (%)
Fe(II) HS	1.264(2)	3.18(4)	0.20(1)	91
Fe(III) HS	0.143*	0.43(4)	0.19(1)	9

[a]Isomer shifts (δ) are given with respect to metallic α-Fe. $\Gamma/2$ = half width of the lines.* fixed parameter.

[2 + 2] Photodimerization of *psca*. Different techniques like vibrational spectroscopy,[34,35] NMR spectroscopy,[36−38] SXRD,[39−41] and AFM[42] have been utilized to monitor the [2 + 2] photodimerization reaction of *trans*-cinnamic acid and its derivatives. Since the reaction is a solid state one, we adhered ourselves mostly toward solid-state characterization techniques. Building on previous research works, we used FT-IR as primary tool to distinguish between the monomer (***psca***) and dimer (***dsta***), which indicated the success of the dimerization reaction. To study the reaction in depth, we used ^{13}C solid state NMR as it has been shown before that solid state NMR spectroscopy not only distinguishes the reactant and product but also provides a sophisticated measure to probe the accurate compositions of monomer and dimer in the reaction mixture at any given time.[38,43,44] Taking advantage of the technique and methodology, we studied photoconversion of ***psca*** into ***dsta*** with respect to time and explained the kinetics of the reaction using the JMAK model of nucleation and growth (see Kinetic Studies section).

Fourier Transform Infrared Spectroscopy. Infrared (IR) spectra of ***psca*** and ***dsta*** over a selected frequencies range are shown in Figure 5. The spectrum of ***psca*** distinctly shows characteristics peaks for sulfonate group and carboxylic group: 1679 cm^{-1} (C═O), 1644 cm^{-1} (C═C), 1311 cm^{-1} (asym S═O), 1123 cm^{-1} (sym S═O), and 824 cm^{-1} (S−O). After irradiation, the spectrum of ***dsta*** does not show any stretching band for C═C bond around 1644 cm^{-1} indicating the completion of the [2 + 2] photodimerization reaction. However, IR spectrum after irradiation shows the presence of all other major bands for sulfonate and carboxylic groups with a slight shifting as compared to ***psca*** suggesting the completion of photodimerization reaction. The noticeable

https://dx.doi.org/10.1021/acs.cgd.0c01149
Cryst. Growth Des. 2020, 20, 7850−7861

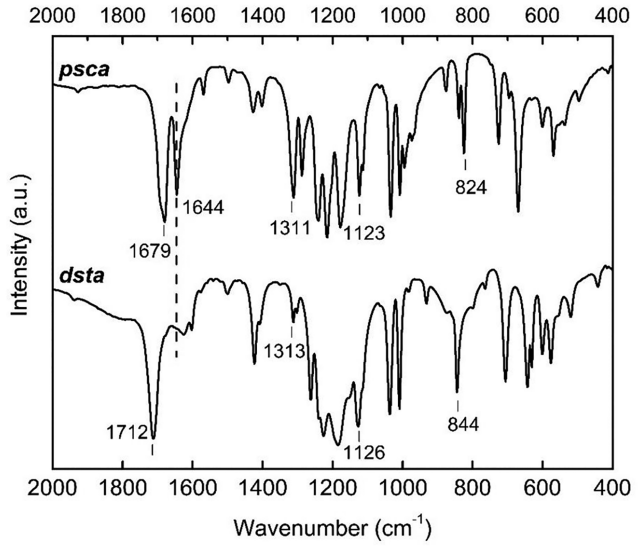

Figure 5. Comparison between IR spectra of ***psca*** (above) and ***dsta*** (below) over a selected range. The dashed line indicates the loss of C═C band after photodimerization in ***dsta***.

bands for ***dsta*** are located at 1712 cm^{-1} (C═O), 1313 cm^{-1} (S═O asym), 1126 cm^{-1} (S═O sym), and 844 cm^{-1} (S−O).

Solid State ^{13}C CP-MAS NMR Spectroscopy. Figure 6 compares the ^{13}C NMR spectra of ***psca*** and ***dsta*** with standard

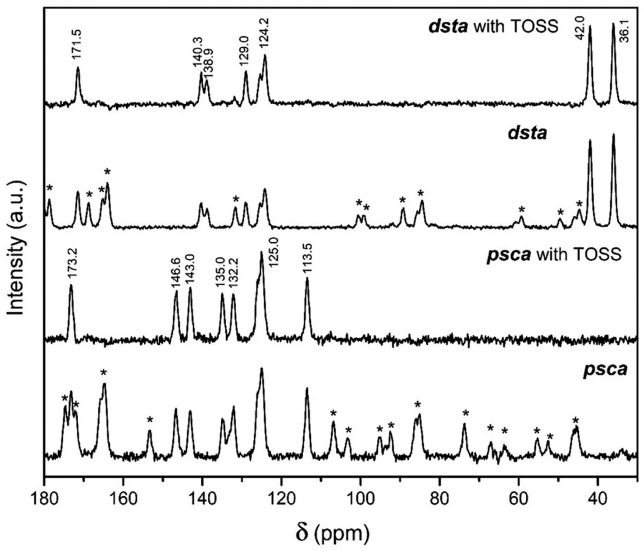

Figure 6. Solid state ^{13}C CP-MAS NMR spectra of ***psca*** and ***dsta*** with and without total suppression of spinning sidebands (TOSS). The asterisks (*) represents the spinning sidebands.

cross-polarization and with total suppression of spinning sidebands (TOSS). Both compounds are clearly distinguishable based on their ^{13}C NMR spectra. The vinylic carbons from ***psca*** resonate at chemical shifts of 143.0 and 113.5 ppm whereas the carbons from phenyl rings give peaks at chemical shift of 146.3, 135.0, 132.2, and 125.0 ppm. On the other hand, the spectrum of ***dsta*** shows two very distinct contributions at 42.0 and 36.1 ppm, corresponding to two carbons from cyclobutane ring. The signals at 140.3, 138.9, 129.0, 124.2 ppm correspond to carbons from two phenyl rings of ***dsta***. The chemical shift of carboxylic carbon is slightly shifted in ***dsta*** relative to ***psca***. It should be noted here that the spectrum of ***dsta*** gives no peaks for vinylic carbons, marking the full completion of the photoconversion. The full assignment of ^{13}C NMR spectra of ***psca*** and ***dsta*** is given in Table 2. The signals are assigned based on the solution state NMR spectra of ***psca*** and ***dsta***. The solution state NMR can be found in the SI (Figure S5, S6, and S7).

Table 2. Solid State ^{13}C CP-MAS NMR Chemical Shift Assignment for *psca* and *dsta*

compound	δ chemical shift (ppm)	
psca	C atoms from phenyl ring:	146.6 (1C), 135.0 (1C) 132.2 (1C), 125.0 (3C)
	C atoms from vinyl chain:	143.0 (1C), 113.5 (1C)
	C atoms from carboxylic:	173.2 (1C)
dsta	C atoms from phenyl rings:	140.3 (2C), 138.9 (2C), 129.0 (2C), 125.4 (2C), 124.2 (4C)
	C atoms from cyclobutane ring:	42.0 (2C), 36.1 (2C)
	C atoms from carboxylic:	171.5 (2C)

Kinetics Study of [2 + 2] Photodimerization. The [2 + 2] photodimerization reaction of ***psca*** was monitored using solid state ^{13}C cross-polarization magic angle spinning (CP-MAS) NMR spectroscopy. The stacked ^{13}C CPMAS NMR spectra of ***psca*** at different irradiation time are shown in Figure 7. Each spectrum is recorded with approximately 100 mg of

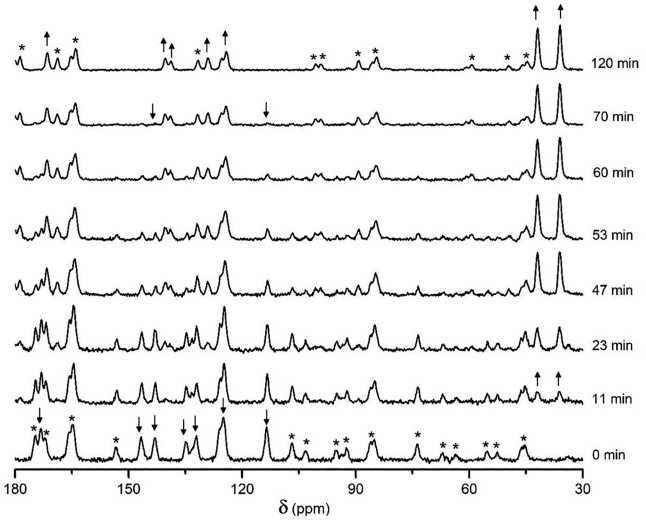

Figure 7. Stacked solid state ^{13}C CP-MAS NMR spectra of photoconversion from ***psca*** to ***dsta*** recorded at different irradiation time. The symbols (↓) and (↑) represent signals from ***psca*** and ***dsta*** respectively, whereas the asterisks (*) represents the spinning sidebands. The irradiation time is written beside each spectrum.

sample, taken after a certain time interval during irradiation. Chemical shifts for ***psca*** and ***dsta*** are marked as (↓) and (↑) respectively. Formation of ***dsta*** is markedly visible in the spectra with signals from cyclobutane carbons started to appear at 42.0 and 36.1 ppm right after the first irradiation. The signals from cyclobutane carbons (↑) become more intense with increasing irradiation time as can be seen in the spectra. On the contrary, the signals from vinylic carbons (↓) at 143.0

https://dx.doi.org/10.1021/acs.cgd.0c01149
Cryst. Growth Des. 2020, 20, 7850−7861

and 113.5 ppm decrease in intensity with increasing irradiation time and disappear after 120 min of irradiation. Signals from phenyl carbons of ***dsta*** are also distinguishable from phenyl carbons of ***psca***, with former's chemical shifts being slightly deshielded.

Figure 8 represents a curve of fractions of ***psca*** converted (into ***dsta***) as a function of time. The degree of conversion is

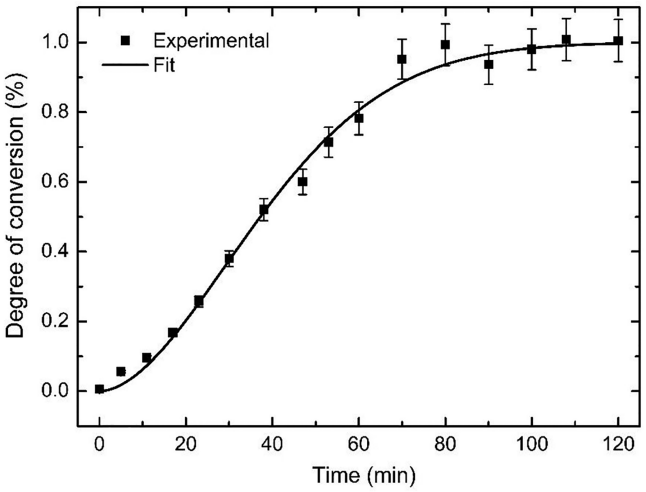

Figure 8. Degree of conversion plot with irradiation time to explain [2 + 2] photoconversion kinetics from ***psca*** to ***dsta***. The curve is fitted according to the JMAK model of nucleation and growth.

evaluated from the ^{13}C CP-MAS NMR spectra using the formula, {integral of cyclobutane signal/(integral of vinyl signal + integral of cyclobutane signal)}. Since the curve obtained is a sigmoidal one, the data was fitted deploying the Johnson–Mehl–Avrami–Kolmogorov (JMAK) model of nucleation and growth in solids.[19−21] The JMAK model has been used before to explain [2 + 2] photodimerization kinetics of *α-trans* cinnamic acid, *β-trans*-cinnamic acid, and a few of their derivatives.[36,43−45] The JMAK equation (commonly known as the Avrami equation) is described as follows:[46,47]

$$y(t) = 1 - \exp(-kt)^n \quad (1)$$

where $y(t)$ represents the fraction of the product formed with time, k is the rate constant, and n represents the order of reaction. Order of the reaction, n determines the type of formation and growth of ***dsta***. Earlier, the JMAK model was developed to describe growth and nucleation for a 3D system where nucleation propagates homogeneously considering the system is infinite and the growth stops at points of mutual contact of newly formed species. However, Weinberg showed that JMAK kinetics can also be applied to explain the growth in a system where nucleation of the new species occurs at the surface[48] very similar to the topochemical photoconversion from ***psca*** to ***dsta***. In case of homogeneous nucleation, Avrami exponent (n) takes an integer value of 4, 3, and 2 for 3D, 2D, and 1D growth, respectively. The JMAK model also comes in handy for the heterogeneous nucleation where n takes fractional values. The heterogeneous nucleation occurs either with a specific rate as the reaction progresses or where a fixed number of nuclei are already present at the onset of reaction. To give an example, suppose n ranges between 1 and 2. If $n \sim 1$ then the nuclei are already present (at the onset of the reaction) in a fixed number, and 1D linear growth occurs rapidly. If $n \sim 2$, nucleation occurs during the course of reaction with a constant rate and growth is 1D linear growth.[36]

Fitting the experimental data according to JMAK kinetics model gives the value of Avrami exponent, $n = 1.8(1)$. The obtained value of n suggests that formation of ***dsta*** occurs through heterogeneous 1-D linear growth. The obtained Avrami exponent is $1 < n < 2$ which suggests that formation of some of the nuclei had occurred at the beginning of the reaction and the rest of the nucleation occurred during the reaction. But because n is more inclined toward 2, this means that the majority of the nucleation occurred during the course of the reaction and the rate at which nucleation occurs, decreases with time. The formation of certain nuclei prior to irradiation might have resulted from exposure to natural sunlight, as was observed by Fonseca et al. for *o*-methoxy cinnamic acid.[43] The presence of certain nuclei at the onset of the reaction and nonuniform nucleation rate with time explains the rapidness of photoconversion at the beginning, and gradual toward the end. Thus, the Avrami exponent, $n = 1.8(1)$, signifies that formation of ***dsta*** occurs by means of heterogeneous 1D linear growth with a decreasing nucleation rate as the reaction proceeds.

DISCUSSION

Our research team has been progressively active in exploring novel photoresponsive hybrid materials based on aromatic anions for the past few years.[2,49−51] The functionalization with a sulfonate group allows the photoresponsive organic compounds to bear a permanent negative charge and which can ease their insertion into inorganic cationic hosts in a controlled manner by the principle of charge neutrality. Proceeding in this direction, we chose to focus on ***psca*** as photoresponsive anion. Its synthesis had to be fully explored since the previous report, dating for almost a century,[27] was not very detailed. We therefore describe in this account the crucial synthetic steps of this photoswitchable salt, for which we also report its photoresponsive properties as well as its structural properties. Indeed, this molecule had never been studied before, except as intermediate reagent in bioorganic chemistry.[52] Since *α*-trans-cinnamic acid has been used and photodimerized in a number of different systems such as diamines double-salt,[9] cocrystals,[11] bile acid conjugates,[12] etc., we therefore anticipate that ***psca*** holds great potential to be photoresponsive in different hosts, e.g. in hybrid inorganic–organic materials or as organic blends. Analysis of the crystal structure of ***psca*** revealed that it qualifies Schmidt's criteria for [2 + 2] photodimerization reaction. We performed the irradiation experiment on a ground sample to have maximum exposure of UV light on the sample. However, we eventually recrystallized ***dsta*** from aqueous acetic acid to obtain single crystals suitable for X-ray diffraction. A powder XRD pattern of ***dsta*** before recrystallization is shown and compared with simulated pattern obtained from single crystal structure of ***dsta*** in Figure S4. The two patterns match very well with each other, implying that recrystallization did not cause any structural changes in ***dsta***. Most interestingly the $P\bar{1}$ space group was preserved in going from ***psca*** to ***dsta***. For the synthesis of $[Fe(H_2O)_6](psca)_2{\cdot}2H_2O$, a novel *in situ* approach was employed which is faster and avoids one extra synthesis step as it does not require ***psca*** to be in the form of sodium salt which is a prerequisite in traditional synthetic approaches for this type of compounds.[22] The synthesis of $[Fe(H_2O)_6](psca)_2{\cdot}2H_2O$ has recently been reported by us,[23] but its

https://dx.doi.org/10.1021/acs.cgd.0c01149
Cryst. Growth Des. 2020, 20, 7850−7861

structural and magnetic properties are described in this paper only. Addition of $FeCl_2·4H_2O$ not only afforded $[Fe(H_2O)_6](psca)_2·2H_2O$ but also neutralized sulfuric acid to form $FeSO_4$. As a result, the reaction mixture was comprised of $FeSO_4$, excess of $FeCl_2$, probably traces of unreacted ***psca*** and the desired product $[Fe(H_2O)_6](psca)_2·2H_2O$. The advantage of using excess of $FeCl_2·4H_2O$ is that it saturates the aqueous solution by $FeSO_4$ and $FeCl_2$ which makes $[Fe(H_2O)_6](psca)_2·2H_2O$ to quickly precipitate out of the reaction mixture. The more soluble $FeSO_4$, $FeCl_2$ and unreacted ***psca*** prefer to stay in the solution phase. Thus, $[Fe(H_2O)_6](psca)_2·2H_2O$ can be easily separated and filtered out without any unwanted impurities.[23]

The crystal structures deserve special attention after detection of oxonium ions in the crystal lattices of ***psca*** and ***dsta***. The crystallization of H_3O^+ salt is indeed a very rare occurrence but not the first instance. In fact, H_3O^+ ions have been seen in the crystal structure of another aromatic sulfonate anion, *p*-toluene sulfonic acid.[53] Hydrogen bonding plays a major role holding ***psca*** in a specific molecular arrangement. If we compare the crystal packing of ***psca*** with its parent molecule, *α-trans*-cinnamic acid, we observe that in the latter, crystal packing consists of pairs of planar molecules which are held together through hydrogen bonds from one carboxylic group to another carboxylic group,[54] whereas in ***psca*** the water molecules of crystallization connects the molecules through a 3D hydrogen bonding network. This is one of the advantages of functionalizing *trans*-cinnamic acid with sulfonate group as it makes ***psca*** soluble in water. Thus, recrystallization of ***psca*** from water allows the H_2O molecules of crystallization to occupy space in the crystal lattice and provides pathways for a 3D hydrogen bonding network as shown in Figure 1d. This specific molecular arrangement for ***psca*** allows the molecules to photodimerize with minimum molecular movement.

The conformation of cyclobutane ring in ***dsta*** was found to be planar. It shows accordance with Margulis' rules for predicting the conformation of cyclobutane ring. These rules predict the conformation based on the substitution of cyclobutane ring. Indeed, if the substitution is centro-symmetrical, the ring will be planar, otherwise, it will have a puckered conformation.[58] Depending on the orientation of substituents on cyclobutane ring, the truxillic acids can be categorized into five different diastereomers, namely alpha (α), epi, peri, gamma (γ), and epsilon (ε) as illustrated in Figure 9.[55] In ***dsta***, the 1,3 and 2,4 substituents on the cyclobutane ring are orientated antiparallel to each other similarly as in alpha type truxillic acid. Moreover, the dihedral and puckering angle of the cyclobutane ring is 0° in ***dsta***, affirming it to be an alpha type truxillic acid. Similar to ***psca***, the sulfonate groups are accountable for the presence of water molecules in ***dsta*** lattice. The hydrogen bonding in ***dsta*** utilizes all the solvent molecules present in the crystal lattice to form a 3D network interconnecting all the truxillic acid molecules. This 3D network structure is very distinct as compared to the previously reported structures of truxillic acid (and derivatives) where hydrogen bonding lead to 1D chains.[56,57] The extended H-bonding network in ***dsta*** is also attributed to the oxygen rich sulfonate and carboxylic groups which occupy the four ends of the molecule. One oxygen atom from each sulfonate groups gets directly involved in H-bonding with neighboring carboxylic groups and the two remaining oxygen atoms of sulfonate groups get involved in H-bonding with solvent molecules which further make hydrogen bonds with neighboring sulfonate and carboxylic groups and so on. The presence of H_2O molecules in lattice of $[Fe(H_2O)_6](psca)_2·2H_2O$ as ligands and solvent molecules results in a 3D hydrogen bonding network which interconnects all the Fe(II) ions. The molecules of ***psca*** provide pathways for H-bonding from both sulfonate and carboxylic group ends. From sulfonate end, oxygen atoms from sulfonate groups make hydrogen bonds with H_2O molecules which in turns is linked to Fe(II) ion. From the carboxylic end, hydrogen atoms from carboxylic groups get involved in hydrogen bonding with oxygen atoms of another carboxylic group from neighboring molecule of ***psca***. This arrangement of hydrogen bonds interconnecting Fe(II) ions is schematically shown in Figure 10.

To date, several characterization techniques have been used to study the kinetics of solid state [2 + 2] photodimerization of *trans*-cinnamic acid (and derivatives). Vibrational spectroscopy monitors the reaction well with respect to time but does not provide structural information on the potential intermediate species,[34,35] contrary to single crystal X-ray diffraction,[40,41] but this latter technique is not suitable for polycrystalline and amorphous powder samples. Another issue lies in the fact that it may interfere with photons in the excitation process and cause X-ray induced [2 + 2] photodimerization to occur,[58,59] though the occurrence of this phenomenon is very rare. Solid state NMR spectroscopy does not interfere however in the [2 + 2] photodimerization and provides precise composition of the reaction mixture at any given time in kinetics study.[36,38,43] Moreover, solid state NMR offers lesser complex option in terms of sample preparation and measurement than single crystal X-ray diffraction. Several factors affect the rate of photodimerization reaction including the UV light intensity as well as the frequency of the mixing/grinding sample during irradiation. The sample quantity is also an important factor: for large quantities of sample, it takes more time to irradiate the entire sample surface and vice versa. Therefore, in order to study the reaction with time, all other variables must be kept constant except irradiation time. Two irradiation methods are recommended: (i) irradiate all the required amount of sample for measurement at once or (ii) irradiate a small amount of sample in equal parts individually for each measurement. In the present work, we have recorded a total of 16 ^{13}C solid state NMR spectra at different irradiation time intervals, working

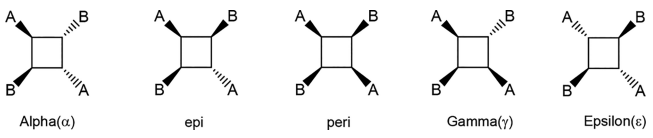

Figure 9. Five possible diastereomers of truxillic acid. In ***dsta***, A = COOH, B = $C_6H_4SO_3$.

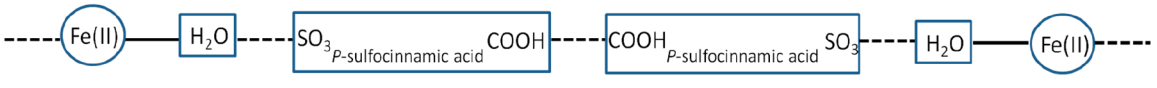

Figure 10. Schematic representation of wave like H-bonding pattern in $[Fe(H_2O)_6](psca)_2·2H_2O$.

https://dx.doi.org/10.1021/acs.cgd.0c01149
Cryst. Growth Des. 2020, 20, 7850−7861

with approximately 100 mg of sample. Given the total amount of sample required for all solid state NMR spectra, we have decided to individually irradiate small amounts of ***psca*** for each spectrum with shuffling every 3 min. Bertmer et al. used the same methodology (solid state ^{13}C NMR spectroscopy and JMAK model) to study the kinetics of [2 + 2] photodimerization of the parent molecule, *α-trans*-cinnamic acid.[36] Their obtained value of Avrami exponent, *n* was of the order of 1.6−1.7 which as a matter of fact is similar to our obtained value of *n* = 1.8. No comparison with any *para*-derivative of *α-trans* cinnamic acid was possible for the kinetics of the photoconversion, due to the absence of any available report. Kinetics study also reveals a 100% photoconversion rate of ***psca*** into ***dsta***. It is indeed an important feature which is not observed for all derivatives of *trans*-cinnamic acid as they are either photostable or undergo only partial photodimerization despite fulfilling Schmidt's topochemical rules.[9,17,60]

CONCLUSIONS

p-Sulfocinnamic acid (***psca***) anion was synthesized and characterized spectroscopically as well as by single crystals X-ray diffraction. The crystal structure revealed ***psca*** to be an *α*-polymorph of *trans*-cinnamic acid which meets the criteria for [2 + 2] photodimerization according to Schmidt's topochemical rules. Such [2 + 2] photodimerization reaction was proven to yield ***dsta***, whose crystal structure revealed a centrosymmetric molecule, which forms a 3D network through hydrogen bonding. The [2 + 2] photodimerization has been carefully monitored using solid state ^{13}C CP-MAS NMR spectroscopy and the kinetics of the reaction was accounted by an heterogeneous 1-D linear growth with a decreasing nucleation rate. Kinetics study also reveals all the molecules of ***psca*** gets converted into ***dsta*** upon irradiation, marking the photoconversion rate as 100%. We successfully inserted ***psca*** into an aqua Fe(II) complex, $[Fe(H_2O)_6](psca)_2{\cdot}2H_2O$. The crystal structure of $[Fe(H_2O)_6](psca)_2{\cdot}2H_2O$ shows accordance with the Schmidt's topochemical rules of [2 + 2] photodimerization. Replacement of ligand water molecules in such aqua complexes by another suitable ligand would allow $[Fe(H_2O)_6](psca)_2{\cdot}2H_2O$ to be a precursor of a number of Fe(II) coordination compounds, for instance nitrogen heterocyclic ligands. In fact, we recently successfully synthesized a neutral coordination complex, incorporated with ***psca***, $[Fe(DMPP)_2(psca)_2]$ (DMPP = dimethyl-1-(2′-pyridyl)-pyrazole) using $[Fe(H_2O)_6](psca)_2{\cdot}2H_2O$ as an intermediate reagent where we replaced six water ligands by two bidentate DMPP ligands and two anionic ***psca*** ligands.[23] This exciting perspective holds a great significance as it opens up an avenue of possibilities to design different Fe based multifunctional compounds, for instance spin crossover compounds,[61] where ***psca*** might provide additional photoresponsive properties to the SCO compounds. This protocol for synthesizing inorganic−organic multifunctional compounds is in fact not restricted to iron but can potentially be utilized to synthesize and explore other metal coordination compounds; given the water solubility provided by the sulfonate group to cinnamic acid, ***psca*** can also be used in cocrystallization.

ASSOCIATED CONTENT

Supporting Information

The Supporting Information is available free of charge at https://pubs.acs.org/doi/10.1021/acs.cgd.0c01149.

Crystallographic information and ORTEP plots of ***psca***, ***dsta***, and $[Fe(H_2O)_6](psca)_2{\cdot}2H_2O$. PXRD of ***dsta*** and solution state NMR spectra of ***psca*** and ***dsta*** (PDF)

Accession Codes

CCDC 2015099−2015101 contain the supplementary crystallographic data for this paper. These data can be obtained free of charge via www.ccdc.cam.ac.uk/data_request/cif, or by emailing data_request@ccdc.cam.ac.uk, or by contacting The Cambridge Crystallographic Data Centre, 12 Union Road, Cambridge CB2 1EZ, UK; fax: +44 1223 336033.

AUTHOR INFORMATION

Corresponding Author

Yann Garcia − *Institute of Condensed Matter and Nanosciences, Molecular Chemistry, Materials and Catalysis (IMCN/MOST), Université catholique de Louvain, 1348 Louvain-la-Neuve, Belgium;* orcid.org/0000-0002-3105-0735; Email: yann.garcia@uclouvain.be

Authors

Varun Kumar − *Institute of Condensed Matter and Nanosciences, Molecular Chemistry, Materials and Catalysis (IMCN/MOST), Université catholique de Louvain, 1348 Louvain-la-Neuve, Belgium*

Luca Fusaro − *Namur Institute of Structured Matter (NISM), Université de Namur, 5000 Namur, Belgium*

Carmela Aprile − *Namur Institute of Structured Matter (NISM), Université de Namur, 5000 Namur, Belgium;* orcid.org/0000-0002-3193-3239

Koen Robeyns − *Institute of Condensed Matter and Nanosciences, Molecular Chemistry, Materials and Catalysis (IMCN/MOST), Université catholique de Louvain, 1348 Louvain-la-Neuve, Belgium*

Complete contact information is available at: https://pubs.acs.org/10.1021/acs.cgd.0c01149

Notes

The authors declare no competing financial interest.

ACKNOWLEDGMENTS

This work was supported by the FNRS (CDR 33694457). This research used resources of the "Plateforme Technologique Physico-Chemical Characterisation" PC^2. Prof. L. Van Meervelt (KULeuven) is thanked for access to his diffractometer for the measurement of ***psca***.

REFERENCES

(1) Szukalski, A.; Korbut, A.; Ortyl, E. Structural and light driven molecular engineering in photochromic polymers. *Polymer* **2020**, *192*, 122311.

(2) Jacquemin, P.-L; Robeyns, K.; Devillers, M.; Garcia, Y. Reversible photochromism of an N-salicylidene aniline anion. *Chem. Commun.* **2014**, *50*, 649−651.

(3) Wang, C.; Li, P.; Zhang, S.; Zhang, G.; Tan, S.; Wu, Y.; Watanabe, M. Azobenzene Molecular Trigger Controlling Phase Transitions of PNIPAm in Ionic Liquids and Light-Controlled Adhesiveness. *Macromolecules* **2020**, *53*, 4901−4907.

(4) Gan, M.-M.; Yu, J.-G.; Wang, Y.-Y.; Han, Y.-F. Template-Directed Photochemical [2 + 2] Cycloaddition in Crystalline Materials: A Useful Tool to Access Cyclobutane Derivatives. *Cryst. Growth Des.* **2018**, *18*, 553−565.

(5) Poplata, S.; Tröster, A.; Zou, Y.-Q.; Bach, T. Recent Advances in the Synthesis of Cyclobutanes by Olefin [2 + 2] Photocycloaddition Reactions. *Chem. Rev.* **2016**, *116*, 9748−9815.

(6) Sonoda, Y. Solid-State [2 + 2] Photodimerization and Photopolymerization of α,ω-Diarylpolyene Monomers: Effective Utilization of Noncovalent Intermolecular Interactions in Crystals. *Molecules* **2011**, *16*, 119−148.
(7) Riiber, C. N. Das directe Ueberführen der Zimmtsäure in α-Truxillsäure. *Ber. Dtsch. Chem. Ges.* **1902**, *35*, 2908−2909.
(8) (a) Cohen, M. C.; Schmidt, G. M. J.; Sonntag, F. I. Topochemistry. Part II. The photochemistry of trans-cinnamic acids. *J. Chem. Soc.* **1964**, 2000−2013. (b) Schmidt, G. M. J. Topochemistry. Part III. The crystal chemistry of some trans-cinnamic acids. *J. Chem. Soc.* **1964**, 2014−2021.
(9) Ito, Y.; Borecka, B.; Trotter, J.; Scheffer, J. R. Control of solid-state photodimerization of trans-cinnamic acid by double salt formation with diamines. *Tetrahedron Lett.* **1995**, *36*, 6083−6086.
(10) Coates, G. W.; Dunn, A. R.; Henling, L. M.; Ziller, J. W.; Lobkovsky, E. B.; Grubbs, R. H. Phenyl−Perfluorophenyl Stacking Interactions: Topochemical [2 + 2] Photodimerization and Photopolymerization of Olefinic Compounds. *J. Am. Chem. Soc.* **1998**, *120*, 3641−3649.
(11) Sarma, J. A. R. P.; Desiraju, G. R. Crystal engineering via Cl ··· Cl non-bonded interactions. The novel 2:1 complex, 6-chloro-3,4-(methylenedioxy)cinnamic acid−2,4-dichlorocinnamic acid. Topochemical conversion into an unsymmetrical cyclobutane and kinetics of the reaction. *J. Chem. Soc., Chem. Commun.* **1984**, 145−147.
(12) Koivukorpi, J.; Kolehmainen, E. UV-induced solvent free synthesis of truxillic acid−bile acid conjugates. *J. Mol. Struct.* **2009**, *930*, 116−120.
(13) Busse, G.; Tschentscher, T.; Plech, A.; Wulff, M.; Frederichs, B.; Techert, S. First investigations of the kinetics of the topochemical reaction of *p*-formyl-trans-cinnamic acid by time-resolved X-ray diffraction. *Faraday Discuss.* **2003**, *122*, 105−117.
(14) Davaasambuu, J.; Busse, G.; Techert, S. Aspects of the Photodimerization Mechanism of 2,4-Dichlorocinnamic Acid Studied by Kinetic Photocrystallography. *J. Phys. Chem. A* **2006**, *110*, 3261−3265.
(15) Schmidt, G. M. J. Photodimerization in the solid state. *Pure Appl. Chem.* **1971**, *27*, 647−678.
(16) Murthy, G. S.; Arjunan, P.; Venkatesan, K.; Ramamurthy, V. Consequences of lattice relaxability in solid state photodimerizations. *Tetrahedron* **1987**, *43*, 1225−1240.
(17) (a) d'Agostino, S.; Spinelli, F.; Boanini, E.; Braga, D.; Grepioni, F. Single crystal to single crystal [2 + 2] photoreactions in chloride and sulphate salts of 4-amino-cinnamic acid via solid-solution formation: a structural and kinetic study. *Chem. Commun.* **2016**, *52*, 1899−1902. (b) d'Agostino, S.; Boanini, E.; Braga, D.; Grepioni, F. Size Matters: [2 + 2] Photoreactivity In Macro- and Microcrystalline Salts of 4-Aminocinnamic Acid. *Cryst. Growth Des.* **2018**, *18*, 2510−2517.
(18) Ramamurthy, V.; Sivaguru, J. Supramolecular Photochemistry as a Potential Synthetic Tool: Photocycloaddition. *Chem. Rev.* **2016**, *116*, 9914−9993.
(19) (a) Avrami, M. Kinetics of Phase Change. I General Theory. *J. Chem. Phys.* **1939**, *7*, 1103−1112. (b) Avrami, M. Kinetics of Phase Change. II Transformation-Time Relations for Random Distribution of Nuclei. *J. Chem. Phys.* **1940**, *8*, 212−224. (c) Avrami, M. Granulation, Phase Change, and Microstructure Kinetics of Phase Change. III. *J. Chem. Phys.* **1941**, *9*, 177−184.
(20) Johnson, W. A.; Mehl, R. F. Reaction kinetics in processes of nucleation and growth. *Am. Inst. Mining. Metall. Eng., Inst. Met. Div. Technol. Publ.* **1939**, *1089*, 1−27.
(21) Kolmogorov, A. N. Zur Statistik der Kristallisationsvorgänge in Metallen. *Bull. Acad. Sci. USSR, Phys. Ser.* **1937**, *1*, 355−359.
(22) Garcia, Y.; van Koningsbruggen, P. J.; Codjovi, E.; Lapouyade, R.; Kahn, O.; Rabardel, L. Non-classical FeII spin-crossover behaviour leading to an unprecedented extremely large apparent thermal hysteresis of 270 K: application for displays. *J. Mater. Chem.* **1997**, *7*, 857−858.
(23) Kumar, V.; El-Massaoudi, M.; Radi, S.; Van Hecke, K.; Rotaru, A.; Garcia, Y. Iron(II) coordination pyrazole complexes with aromatic sulfonate ligands: the role of ether. *New J. Chem.* **2020**, *44*, 13902−13912.
(24) *CrysAlisPro*, CrysAlisPro Software system, Version 1.171.37.35; Agilent Technologies, 2014.
(25) Sheldrick, G. M. SHELXT − Integrated space-group and crystal-structure determination. *Acta Crystallogr., Sect. A: Found. Adv.* **2015**, *A71*, 3−8.
(26) Sheldrick, G. M. Crystal structure refinement with SHELXL. *Acta Crystallogr., Sect. C: Struct. Chem.* **2015**, *C71*, 3−8.
(27) Moore, F. J.; Tucker, G. R. A renewed study of the sulfonation of cinnamic acid: A new proof that the secondary product is meta-sulfocinnamic acid; Synthesis of the true ortho-sulfocinnamic acid, and the action of sodium bisulfite upon cinnamic acid derivatives. *J. Am. Chem. Soc.* **1927**, *49*, 258−266.
(28) Margulis, T. N. Structure of a Planar Cyclobutane. *cis,trans,cis*-1,2,3,4-Cyclobutanetetracarboxylic Acid Tetramethyl Ester. *J. Am. Chem. Soc.* **1971**, *93*, 2193−2195.
(29) Robinson, K.; Gibbs, G. V.; Ribbe, P. H. Quadratic Elongation: A Quantitative Measure of Distortion in Coordination Polyhedra. *Science* **1971**, *172*, 567−570.
(30) Xue, S.; Guo, Y.; Rotaru, A.; Müller-Bunz, H.; Morgan, G. G.; Trzop, E.; Collet, E.; Olah, J.; Garcia, Y. Spin Crossover Behavior in a Homologous Series of Iron(II) Complexes Based on Functionalized Bipyridyl Ligands. *Inorg. Chem.* **2018**, *57*, 9880−9891.
(31) Lagarec, K.; Rancourt, D. G. *Recoil*, Mössbauer Spectral Analysis Software for Windows 1.0; Department of Physics, University of Ottawa, Canada, 1998.
(32) Gütlich, P.; Garcia, Y. Mössbauer Spectroscopy: Elegance and Versatility in Chemical Diagnostics. *J. Phys. Conf. Ser.* **2010**, *217*, 012001.
(33) DeBenedetti, S.; Lang, G.; Ingalls, R. Electric quadrupole splitting and the nuclear volume effect in the ions of Fe^{57}. *Phys. Rev. Lett.* **1961**, *6*, 60−62.
(34) Allen, S. D. M.; Almond, M. J.; Bruneel, J. L.; Gilbert, A.; Hollins, P.; Mascetti, J. The photodimerisation of trans-cinnamic acid and its derivatives: a study by vibrational microspectroscopy. *Spectrochim. Acta, Part A* **2000**, *56*, 2423−2430.
(35) Jenkins, S. L.; Almond, M. J.; Atkinson, S. D.M.; Drew, M. G. B.; Hollins, P.; Mortimore, J. L.; Tobin, M. J. The kinetics of the 2π+2π photodimerisation reactions of single-crystalline derivatives of trans-cinnamic acid: A study by infrared microspectroscopy. *J. Mol. Struct.* **2006**, *786*, 220−226.
(36) Bertmer, M.; Nieuwendaal, R. C.; Barnes, A. B.; Hayes, S. E. Solid-State Photodimerization Kinetics of α-*trans*-Cinnamic Acid to α-Truxillic Acid Studied via Solid-State NMR. *J. Phys. Chem. B* **2006**, *110*, 6270−6273.
(37) Khoj, M. A.; Hughes, C. E.; Harris, K. D. M.; Kariuki, B. M. Polymorphism in a *trans*-Cinnamic Acid Derivative Exhibiting Two Distinct β-type Phases: Structural Properties, [2 + 2] Photodimerization Reactions, and Polymorphic Phase Transition Behavior. *Cryst. Growth Des.* **2013**, *13*, 4110−4117.
(38) Fonseca, I.; Hayes, S. E.; Blümich, B.; Bertmer, M. Temperature stability and photodimerization kinetics of β-cinnamic acid and comparison to its α-polymorph as studied by solid-state NMR spectroscopy techniques and DFT calculations. *Phys. Chem. Chem. Phys.* **2008**, *10*, 5898−5907.
(39) Enkelmann, V.; Wegner, G.; Novak, K.; Wagener, K. B. Single-crystal-to-single-crystal photodimerization of cinnamic acid. *J. Am. Chem. Soc.* **1993**, *115*, 10390−10391.
(40) Fernandes, M. A.; Levendis, D. C. Photodimerisation of the α′-polymorph of ortho-ethoxy-trans-cinnamic acid occurs via a two-stage mechanism at 343 K yielding 100% α-truxillic acid. *CrystEngComm* **2016**, *18*, 7363−7376.
(41) d'Agostino, S.; Taddei, P.; Boanini, E.; Braga, D.; Grepioni, F. Photo- vs Mechano-Induced Polymorphism and Single Crystal to Single Crystal [2 + 2] Photoreactivity in a Bromide Salt of 4-Amino-Cinnamic Acid. *Cryst. Growth Des.* **2017**, *17*, 4491−4495.

https://dx.doi.org/10.1021/acs.cgd.0c01149
Cryst. Growth Des. 2020, 20, 7850−7861

(42) Kaupp, G. Photodimerization of Cinnamic Acid in the Solid State: New Insights on Application of Atomic Force Microscopy. *Angew. Chem., Int. Ed. Engl.* **1992**, *31*, 592−595.
(43) Fonseca, I.; Hayes, S. E.; Bertmer, M. Size effects of aromatic substitution in the ortho position on the photodimerization kinetics of α-transcinnamic acid derivatives. A solid-state NMR study. *Phys. Chem. Chem. Phys.* **2009**, *11*, 10211−10218.
(44) Fonseca, I.; Baias, M.; Hayes, S. E.; Pickard, C. J.; Bertmer, M. Effects of Aromatic Substitution on the Photodimerization Kinetics of β-trans Cinnamic Acid Derivatives Studied with 13C Solid-State NMR. *J. Phys. Chem. C* **2012**, *116*, 12212−12218.
(45) Panda, T.; Naumov, P. Time-Dependent Photodimerization of α-trans-Cinnamic Acid Studied by Photocalorimetry and NMR Spectroscopy. *Cryst. Growth Des.* **2018**, *18*, 2744−2749.
(46) Kohout, J. An alternative to the JMAK equation for a better description of phase transformation kinetics. *J. Mater. Sci.* **2008**, *43*, 1334−1339.
(47) Bąkowicz, J.; Olejarz, J.; Turowska-Tyrk, I. Steering photochemical reactivity of2,4,6-triisopropylbenzophenonate anion in a crystalline state. *J. Photochem. Photobiol., A* **2014**, *273*, 34−42.
(48) Weinberg, M. C. Time-Dependent Photodimerization of α-trans-Cinnamic Acid Studied by Photocalorimetry and NMR Spectroscopy. *J. Non-Cryst. Solids* **1991**, *134*, 116−122.
(49) (a) Robert, F.; Naik, A. D.; Garcia, Y. Influence of a thermochromic anion on the spin crossover of iron(II) trinuclear complexes probed by Mössbauer spectroscopy. *J. Phys. Conf. Ser.* **2010**, *217*, 012031. (b) Robert, F.; Naik, A. D.; Garcia, Y. *N*-salicylidene aniline derivatives as emerging solid-state molecular switches towards multifunctional organic-inorganic architectures. *Möss. Eff. Ref. Data J.* **2011**, *34*, 199−203. (c) Robert, F.; Naik, A. D.; Tinant, B.; Garcia, Y. *N*-Salicylidene anil anions as thermosensitive components of organic−inorganic hybrid materials. *Inorg. Chim. Acta* **2012**, *380*, 104−113.
(50) Jacquemin, P. L.; Garcia, Y.; Devillers, M. Blends made from *N*-salicylidene aniline sulfonate derivatives and a polyampholyte matrix: in situ synthesis vs. solution mixing. *J. Mater. Chem. C* **2014**, *2*, 1815−1822.
(51) Jacquemin, P. L.; Robeyns, K.; Devillers, M.; Garcia, Y. Photochromism Emergence in *N*-Salicylidene *p*-Aminobenzenesulfonate Diallylammonium Salts. *Chem. - Eur. J.* **2015**, *21*, 6832−6845.
(52) Müller, C. E.; Sandoval-Ramírez, J.; Schobert, U.; Geis, U.; Frobenius, W.; Klotz, K. N. 8-(Sulfostyryl)xanthines: water-soluble A2A-selective adenosine receptor antagonists. *Bioorg. Med. Chem.* **1998**, *6*, 707−719.
(53) Arora, S. K.; Sundaralingam, M. The crystal and molecular structure of 4-methyl sulfonic acid (p-toluenesulfonic acid) monohydrate, $C_7H_8SO_3$-.H_3O^+, an oxonium salt. *Acta Crystallogr., Sect. B: Struct. Crystallogr. Cryst. Chem.* **1971**, *B27*, 1293−1298.
(54) Wierda, D. A.; Feng, T. L.; Barron, A. R. Structure of α-*trans*-cinnamic acid. Addendum. *Acta Crystallogr., Sect. C: Cryst. Struct. Commun.* **1989**, *C45*, 338−339.
(55) Berg, U.; Rappoport, Z.; Liebman, J. F. Stereochemical Aspects—Conformation and Configuration. *Chemistry of Cyclobutanes* **2005**, 83.
(56) Mishra, M. K.; Mukherjee, A.; Ramamurty, U.; Desiraju, G. R. Crystal chemistry and photomechanical behavior of 3,4-dimethoxycinnamic acid: correlation between maximum yield in the solid-state topochemical reaction and cooperative molecular motion. *IUCrJ* **2015**, *2*, 653−660.
(57) Abdelmoty, I.; Buchholz, V.; Di, L.; Guo, C.; Kowitz, K.; Enkelmann, V.; Wegner, G.; Foxman, B. M. Polymorphism of Cinnamic and α-Truxillic Acids: New Additions to an Old Story. *Cryst. Growth Des.* **2005**, *5*, 2210−2217.
(58) Ohba, S.; Ito, Y. Single-crystal-to-single-crystal photodimerization of 4-chlorocinnamoyl-O,O′-dimethyldopamine. *Acta Crystallogr., Sect. B: Struct. Sci.* **2003**, *B59*, 149−155.
(59) Inkinen, J.; Niskanen, J.; Talka, T.; Sahle, C. J.; Müller, H.; Khriachtchev, L.; Hashemi, J.; Akbari, A.; Hakala, M.; Huotari, S. X-ray induced dimerization of cinnamic acid: Time-resolved inelastic X-ray scattering study. *Sci. Rep.* **2015**, *5*, 15851.
(60) Lei, T.; Zhou, C.; Huang, M.-Y.; Zhao, L.-M.; Yang, B.; Ye, C.; Xiao, H.; Meng, Q.-Y.; Ramamurthy, V.; Tung, C.-H.; Wu, L.-Z. General and Efficient Intermolecular [2 + 2] Photodimerization of Chalcones and Cinnamic Acid Derivatives in Solution through Visible-Light Catalysis. *Angew. Chem., Int. Ed.* **2017**, *56*, 15407−15410.
(61) Gütlich, P.; Gaspar, A. B.; Garcia, Y. Spin state switching in iron coordination compounds. *Beilstein J. Org. Chem.* **2013**, *9*, 342−391.

https://dx.doi.org/10.1021/acs.cgd.0c01149
Cryst. Growth Des. 2020, 20, 7850−7861